White Rose Research Online

eprints@whiterose.ac.uk
https://eprints.whiterose.ac.uk
Universities of Leeds, Sheffield and York

Deposited via The University of Leeds.

White Rose Research Online URL for this paper:
https://eprints.whiterose.ac.uk/id/eprint/203735/

Version: Accepted Version

Article:
Lyu, P., Luo, Q., Wang, T. et al. (2023) Railway gravity retaining wall design using the flower pollination algorithm. Transportation Geotechnics, 42. 101065. ISSN: 2214-3912

https://doi.org/10.1016/j.trgeo.2023.101065

© 2023, Elsevier. This manuscript version is made available under the CC-BY-NC-ND 4.0 license http://creativecommons.org/licenses/by-nc-nd/4.0/.

Reuse
This article is distributed under the terms of the Creative Commons Attribution-NonCommercial-NoDerivs (CC BY-NC-ND) licence. This licence only allows you to download this work and share it with others as long as you credit the authors, but you can't change the article in any way or use it commercially. More information and the full terms of the licence here: https://creativecommons.org/licenses/

Takedown
If you consider content in White Rose Research Online to be in breach of UK law, please notify us by emailing eprints@whiterose.ac.uk including the URL of the record and the reason for the withdrawal request.

UNIVERSITY OF LEEDS
University of Sheffield
UNIVERSITY of York

Railway Gravity Retaining Wall Design Using the Flower Pollination Algorithm

Pengju Lyu

School of Civil Engineering, Southwest Jiaotong Univ., Chengdu 610031, China

E-mail: 1026279332@qq.com

Qiang Luo

School of Civil Engineering, Southwest Jiaotong Univ., Chengdu 610031, China;

MOE Key Laboratory of High-speed Railway Engineering, Southwest Jiaotong Univ., Chengdu 610031, China

E-mail: lqrock@swjtu.edu.cn

Tengfei Wang*

School of Civil Engineering, Southwest Jiaotong Univ., Chengdu 610031, China;

MOE Key Laboratory of High-speed Railway Engineering, Southwest Jiaotong Univ., Chengdu 610031, China

E-mail: w@swjtu.edu.cn (*Corresponding author)

ORCID: 0000-0003-4079-0687

David P. Connolly

School of Civil Engineering, University of Leeds, Leeds LS2 9JT, UK

Email: D.Connolly@leeds.ac.uk

Abstract

An optimized cross-sectional area of a retaining wall assists in reducing material costs. Nevertheless, the design solution obtained from the traditional methods is not always the optimal one. Therefore, this study uses the flower pollination algorithm (FPA) to optimize the configuration of a gravity retaining wall, attempting to find the smallest cross-sectional area that meets design requirements. A key novelty is the use of a metaheuristic for gravity retaining wall design considering railway loading. First, the FPA is described in detail along with the general design methods for retaining walls and the definition of the optimisation problem. Next, a gravity retaining wall case study is performed and the FPA method is compared against alternative genetic algorithm (GA), particle swarm optimization (PSO), and other approaches. Lastly, a parametric analysis is performed to assess the impact of the design parameters on the optimization outcomes. Results indicate that the FPA furnishes an effective methodology for optimizing the design of gravity retaining walls when switch probability values oscillate between 0.1 and 0.8, the population comprises 20 individuals, the constant of the Lévy flight step size lies between 1 and 2, and the Lévy flight step size scale factor ranges from 0.001 to 0.1. Further, the consistency of the algorithm's results and its convergence rate present a significant advantage over alternate algorithms. The evidence posits that implementing a landward-leaning wall back with an inclination angle of 14.04° facilitates the attainment of the optimal minimum cross-sectional area. The wall height emerges as the predominant determinant of the minimum cross-sectional area, demonstrating negligible sensitivity to ground bearing capacities exceeding 300 kPa. Finally, the algorithm is shown to be capable of identifying the design requirement thresholds for which retaining walls are unviable (e.g. ground bearing capacity being 100 kPa or the wall height exceeding

7 m), and for which alternative designs should be explored.

Keywords: Optimum Design; Gravity Retaining Walls; Railway Embankments; Flower Pollination Algorithm

1 Introduction

The railway is one of the most important means of transport [1,2]. And its roadbed is a significant structure situated below the railway track system, primarily constructed from natural soil and stone materials[3]. Compared to other engineering structures such as bridges, tunnels, and culverts, the roadbed has lower construction difficulty, engineering risk, and construction costs [4]. Embankments of soil and stone fill can be used directly to form parts of the roadbed where the surface is higher than the ground, and a slope with a certain gradient is built beyond the shoulder edge to ensure stability for the general embankment. Replacing the soil beneath a slope with a retaining structure can save the embankment footprint and reduce the amount of fill required. Gravity retaining walls are a much-favoured type of retaining structure in civil and railway engineering due to their simple construction and ease of building. These walls rely on their own weight to resist the earth pressure behind them and prevent soil collapse and slipping. The cross-section design can be obtained from a given set of drawings or tables, or it can be drafted based on engineering experience, followed by an examination of the stability and strength [5]. Nevertheless, the design solution thus obtained presents challenges in ensuring that the retaining wall has the minimum cross-sectional area while satisfying the design requirements.

Owing to the pervasive utilization of railway gravity retaining walls [6], even slight alterations in their cross-sectional configuration can yield substantial savings in terms of wall materials. Consequently, a prudent selection of the minimum cross-sectional area can effectively optimize material utilization and significantly bolster the economic efficiency entwined with material costs, thereby bearing considerable significance in the realm of railway construction. Furthermore, the

essential materials necessary for the fabrication of retaining walls, such as concrete and cement, are deemed carbon-intensive commodities. Similarly, the extensive transportation of materials and on-site construction activities entail carbon-intensive process [7]. Thus, reducing material consumption contributes to the mitigation of carbon emissions and the lessening of ecological repercussions associated with construction activities. This aspect assumes paramount significance in the realm of environmental conservation and the promotion of sustainable development. Henceforth, it is of utmost importance to employ a methodology that discerns the optimal design solution for railway gravity retaining wall, one that not only satisfies the design criteria but also embodies the smallest cross-sectional area.

Metaheuristic algorithms, such as cuckoo search (CS) [8], firefly algorithm (FA) [9], genetic algorithm (GA) [10], particle swarm optimization (PSO) [11], shuffled shepherd optimization algorithm (SSOA) [12], tug of war optimization (TWO) [13], charged system search (CSS) [14], and flower pollination algorithm (FPA) [15], can be applied in the design of engineering structures. These algorithms often consider the requirements to ensure the safety of structure as constraints, the construction costs such as material usage as objective functions, and the structural dimensions and spatial locations as design variables. This then helps engineers search for combinations of design variables that satisfy the constraints and minimise the value of the objective function. For instance, Kaveh and Mahdavi [16] utilized three algorithms, namely CSS, PSO, and a hybrid CSS and PSO (CSS-PSO), to investigate the optimal design solution for minimizing the construction cost or concrete volume of double curvature arch dams under seismic loading conditions. Metaheuristic optimization methods have also been employed in the realm of retaining wall design. For example, multiple

algorithms have been utilized to design cantilever retaining walls [17–22]. For gravity retaining walls, Varga et al. [23] used a real coded genetic algorithm (RCGA) to optimize the design considering the total cost of material, excavation, filling, and drainage as the objective function. Talatahari et al. [24] used the CSS algorithm to search for the optimum design of gravity retaining walls subject to seismic loads, using the self-weight of the wall as the objective function. In addition, Kaveh and Zakian [25] explored the optimal shape corresponding to the minimum cross-sectional area using various algorithms such as CSS for concrete gravity dams similar to gravity retaining walls that rely on self-weight to maintain the stability of the system.

Inspired by the pollination process of flowers in nature, Yang [15] proposed a population-based FPA metaheuristic algorithm. The algorithm amalgamates robust local and global search capabilities while exhibiting exceptional convergence speed. And it is advantageous compared to some other metaheuristic algorithms due to its ease of implementation, high efficiency, and adaptability. Notably, it has proven to be efficacious in tackling optimization problems within diverse scientific fields [26], such as image processing [27,28], power systems [29,30], structures [31] and geotechnical engineering [20,22,32,33]. Related to geotechnical engineering, Singh et al. [32] and ÖCAL et al. [33] proposed the use of FPA to search for the location of critical sliding surfaces for slope stability analysis, while Mergos and Mantoglou [20] and YÜCEL et al. [22] used FPA for the design of cantilever retaining walls.

Upon considering the preceding discourse, an endeavour is undertaken to optimize the design of the gravity retaining wall of railway embankment utilizing FPA, with the aim of acquiring the optimum design that satisfies the design requisites while possessing the minimum cross-sectional area. An initial

exploratory study is carried out to demonstrate the advantages of the FPA over traditional design methods and to determine the optimal FPA parameter values that would produce the highest level of performance in gravity retaining wall design. Furthermore, a comparative study with established algorithms, such as GA, PSO, SSOA, and TWO is being performed to further assess its performance. Finally, a parametric study is conducted to demonstrate the effects of parameters associated with usage scenarios on the optimization results. These research findings can serve as a reference for the design of gravity retaining wall supporting railway embankment.

2 Methodology

This section provides a detailed description of the FPA and the general design methods for railway retaining walls. Following this, the optimization problem is stated.

2.1 Flower pollination algorithm

FPA, which is formed based on the analogy of flower pollination, has been utilized in contemporary civil engineering optimization applications. Pollen transfer in natural plants can be accomplished by either cross-pollination or self-pollination. Cross-pollination is predominantly achieved by biological pollination, in which biological pollinators like insects and birds transport pollen over considerable distances between plants. These animal pollinators are inclined to ignore other flower species and exclusively visit particular flower species, resulting in what is commonly known as “flower constancy” [34]. On the other hand, self-pollination is mainly achieved through abiotic pollination, wherein wind or water carries pollen between different flowers or the same flower. The aforementioned characteristics of flower pollination are defined by the following rules [15]:

a. Cross-pollination is considered as global pollination, where the pollen-carrying pollinators

make a Lévy flight;

b. Self-pollination is viewed as local pollination;

c. Flower constancy can be regarded as the probability of reproduction, proportional to the similarity of the two flowers involved in the pollination process.

d. Global or local pollination is determined by a switch probability p that is a pre-fixed constant in [0,1].

In the process of FPA, a group of candidate solution vectors X_1, X_2, …, X_i, …, X_{npop} simulates a population comprising n_{pop} flowers. The next-generation solution vector is created by applying global or local pollination operations to X_i. Mathematically, the combination of global pollination (rule a) and flower constancy (rule c) can be expressed as:

$$X_i^{t+1} = X_i^t + \gamma L(\lambda)\left(g_* - X_i^t\right) \tag{1}$$

where X_i^t denotes the solution vector X_i at iteration t, g_* signifies the best solution of the current iteration, γ represents the scaling factor controlling the step size, and λ is a constant of $L(\lambda)$ for which Yang [15] recommends a value of 3/2. $L(\lambda) > 0$ denotes the Lévy flight step size.

Moreover, local pollination (rule b) coupled with flower constancy (rule c) can be mathematically represented as:

$$X_i^{t+1} = X_i^t + \varepsilon\left(X_j^t - X_k^t\right) \tag{2}$$

where X_j^t, X_k^t is a randomly chosen solution vector from the set of solution vectors at iteration t, and ε is a random number chosen from a uniform distribution in [0, 1].

If a random number generated from the interval [0, 1] is smaller than the switch probability p specified in rule d, then global pollination is used to generate a new solution vector. Otherwise, local

pollination is carried out. Yang [15] has shown that a value of p = 0.8 typically produces acceptable results. The FPA pseudo-code is depicted in Fig. 1.

Flower Pollination Algorithm

Determine the objective function f(X), $X = (x_1, x_2, \ldots, x_{\text{dim}})$
Initialize a population of n_{pop} flowers
Find the best solution g_* of the initial population
Set the value switch probability $p \in [0, 1]$
while (t < Maximum iterations)
  for i = 1:n_{pop} (for all n_{pop} flowers in the population)
    if rand < p
      Draw a dim-dimensional vector L from a Lévy distribution
      Global pollination by $X_i^{t+1} = X_i^t + \gamma L(\lambda)(g_* - X_i^t)$.
    else
      Draw ε value from a uniform distribution in [0, 1]
      Local pollination by $X_i^{t+1} = X_i^t + \varepsilon(X_j^t - X_k^t)$
    end if
    Caculate and evaluate objective function values of new solutions
    If better, update new solutions in the population
  end for
  Find the current best solution g_* in new population
end while
Output the best solution and its objective function value

Fig. 1 Pseudo-code of FPA

2.2 Methods for retaining wall design

The longitudinal extent of a retaining wall that provides support to a embankment considerably surpasses its cross-sectional dimensions, thereby enabling the simplification of its stability analysis as a problem of plane strain [35]. Fig. 2 illustrates a typical stability analysis diagram of a gravity retaining wall supporting a railway embankment. In Fig. 2a, the gravity retaining wall is depicted as having a height denoted H, with a top width of b, a wall face slope of 1:n, a wall back inclination angle of α, and a bottom surface width of B which is set at an angle of α_o with respect to the horizontal. The height of the wall toe from the subgrade surface is indicated by H_s, while the height and width of the

wall toe step are specified as h_1 and b_1, respectively. Additionally, the face of the wall toe step is arranged in parallel with the wall face. In engineering practice, a slope of embankment with a height of h and a slope gradient of 1:1.5 is often set above the wall top. The line spacing of a double-track railway is denoted as D. The distance from the center of the track near retaining wall to the top of wall back is indicated as d_s, while the distance to the edge of embankment shoulder is designated as d.

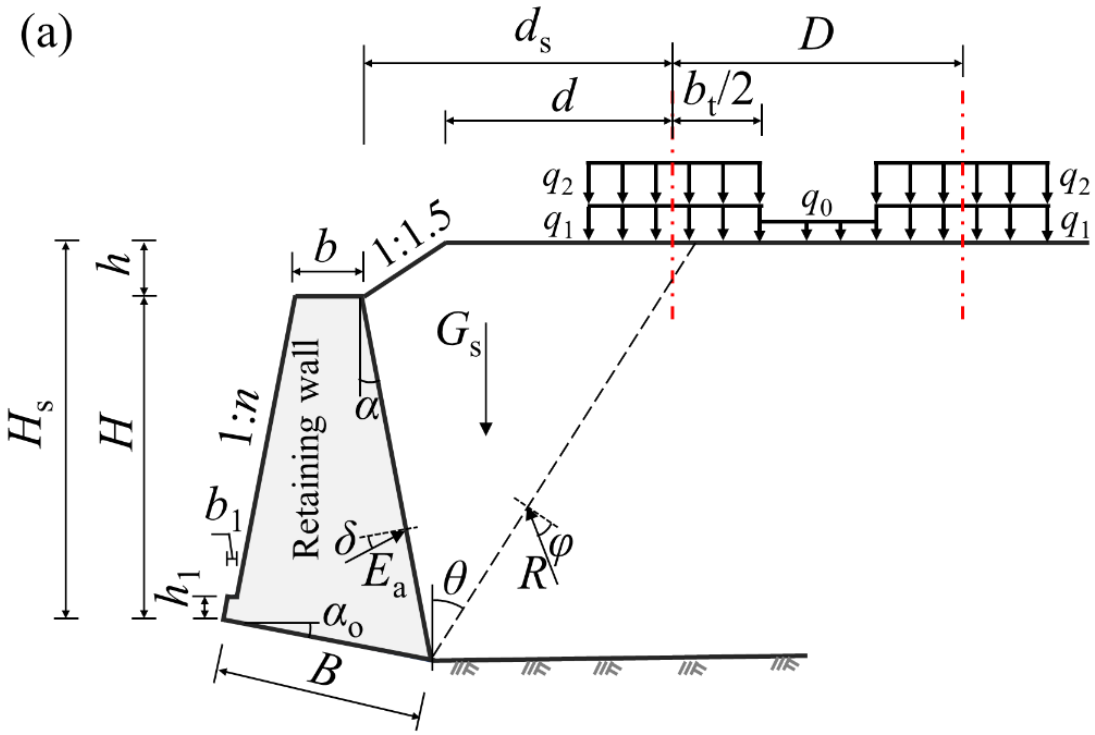

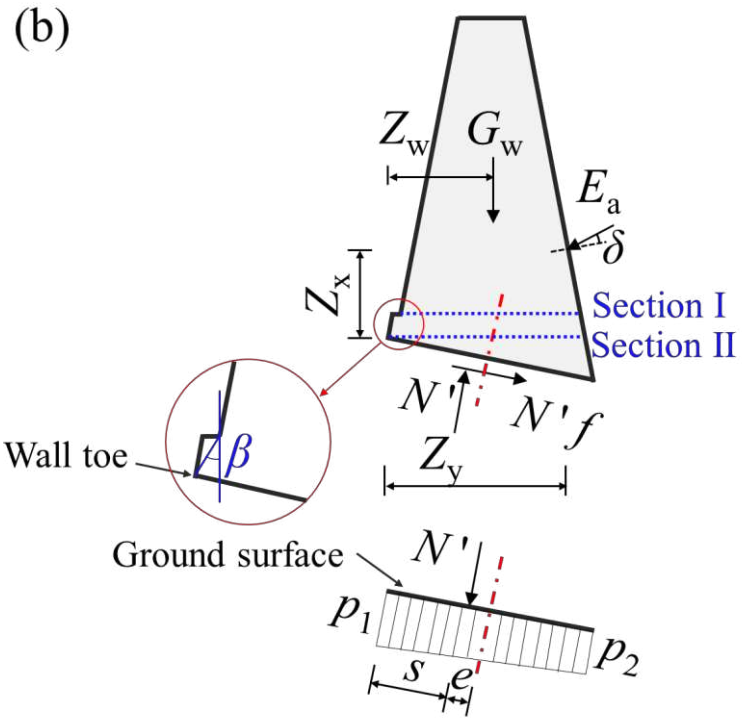

Fig. 2 Stability analysis diagram of gravity retaining wall supporting railway embankment: (a) geometry of embankment and force analysis of soil wedge behind the wall; (b) force analysis of gravity retaining wall

For stability analysis, the track load, train load and the load between two tracks are simplified as a uniformly distributed load on the crest due to self-weight of imaginary fill. These loads are denoted as q_1, q_2 and q_0 in Fig. 2a, and the distribution widths of q_1 and q_2 are represented by b_t. Also, in Fig. 2a, the sliding wedge behind the wall, corresponding to the active limit equilibrium state, is determined by the earth pressure theory of Coulomb and is subject to the self-weight G_s, the active earth pressure E_a at the back of the wall, and the stable soil reaction force R. θ denotes the angle between the sliding surface and the vertical surface, while δ refers to the angle between E_a and the normal to the wall back (i.e. the wall-soil friction angle), and φ represents the angle between R and the normal to the sliding surface (i.e. the friction angle of the fill). In the design of retaining walls with shallow foundations, the passive earth pressure in front of the wall may be disregarded.

Fig. 2b illustrates the forces exerted on the retaining wall and the stress distribution at its bottom surface. Stability analysis is conducted in accordance with the *Code for Design of Retaining Structures of Railway Earthworks* (TB10025-2019), which involves evaluating anti-slip stability, anti-overturning stability, eccentricity and the compressive stress under the foundation. The anti-slip stability coefficients, K_c and K_c', are determined using Eq. 3 and Eq. 4respectively, while the anti-overturning stability coefficient, K_0, is calculated using Eq. 5. K_c pertains to the potential slip surface along the bottom surface of the retaining wall, while K_c' corresponds to the potential slip surface along the horizontal plane where the wall heel is located.

$$K_c = \frac{N'f}{E_a \cos(\alpha+\delta+\alpha_o) - G_w \sin\alpha_o} = \frac{[G_w \cos\alpha_o + E_a \sin(\alpha+\delta+\alpha_o)]f}{E_a \cos(\alpha+\delta+\alpha_o) - G_w \sin\alpha_o} \tag{3}$$

$$K_c' = \frac{\left[G_w + E_y + 0.5\gamma_g B^2 \cos\alpha_o \sin\alpha_o\right] f'}{E_x} \tag{4}$$

$$K_0 = \frac{G_w Z_w + E_y Z_y}{E_x Z_x} \tag{5}$$

where G_w is the self-weight of wall, E_x and E_y denote the horizontal and vertical components of active earth pressure E_a acting behind the wall. Meanwhile, Z_w, Z_x and Z_y refer to the arm length of the moment created by G_w, E_x and E_y at the wall toe, respectively. N' represents the normal force acting on the wall base, f is the friction coefficient of the wall-ground. γ_g, f' are the weight and the coefficient of friction of the ground soil respectively.

The eccentricity e is determined using Eq. 6. Additionally, the compressive stress at the toe and heel of the wall (denoted by p_1 and p_2 respectively), and the average compressive stress p_m under base, are calculated using Eq. 7 to Eq. 10.

$$e = \frac{B}{2} - s = \frac{B}{2} - \frac{\left(G_{\mathrm{w}} Z_{\mathrm{w}} + E_{\mathrm{y}} Z_{\mathrm{y}} - E_{\mathrm{x}} Z_{\mathrm{x}}\right)}{N'} \tag{6}$$

$$p_{1,2} = \frac{N'}{B}\left(1 \pm \frac{6e}{B}\right), \text{ if } |e| \le \frac{B}{6} \tag{7}$$

$$p_1 = \frac{2N'}{3s}, p_2 = 0, \text{ if } e > \frac{B}{6} \tag{8}$$

$$p_1 = 0, \ p_2 = \frac{2N'}{3(B-s)}, \text{ if } e < \frac{-B}{6} \tag{9}$$

$$p_m = \frac{p_1 + p_2}{2} \tag{10}$$

where s denotes the moment arm length created by N' at the wall toe.

In addition to conducting a stability analysis, it is also important to evaluate the strength of the retaining wall. As shown in Fig. 2b, Sections I and II, denoting the horizontal section where the top and bottom of the wall toe step are situated, are selected as representative sections for strength evaluation. The eccentricity e_1 of the section is evaluated according to Eq. 11, and the tensile and compressive stresses in the normal direction are assessed using Eq. 12. When $|e_1| > B_1/6$, the outcomes of Eq. 12 contain negative value, indicating that tensile stress occurs in the normal direction of the section. It is essential to ensure that the tensile stress is less than the allowable bending tensile strength $[\sigma_t]$ of the material. Additionally, the maximum compressive stress σ_{max} of the section after stress redistribution should be evaluated using Eq. 13. The shear stress τ is calculated using Eq. 14 and $\left(G_{1\mathrm{w}} + E_{1\mathrm{y}}\right) f_1$ as resistance can safely be omitted. Finally, note that the wall sections are evaluated approximately by the earth pressure applied to the entire back of the wall.

$$e_1 = B_1/2 - (G_{1\mathrm{w}} Z_{1\mathrm{w}} + E_{1\mathrm{y}} Z_{1\mathrm{y}} - E_{1\mathrm{x}} Z_{1\mathrm{x}}) \big/ (G_{1\mathrm{w}} + E_{1\mathrm{y}}) \tag{11}$$

$$\sigma_{1,2} = \frac{(G_{1\mathrm{w}} + E_{1\mathrm{y}})}{B_1}\left(1 \pm \frac{6e_1}{B_1}\right) \tag{12}$$

$$\sigma_{\max}=\begin{cases}2(G_{1w}+E_{1y})/3(B_1/2-e_1), & e_1>B_1/6\\ 2(G_{1w}+E_{1y})/3(B_1/2+e_1), & e_1<-B_1/6\end{cases} \tag{13}$$

$$\tau=(E_{1x}-(G_{1w}+E_{1y})f_1)/B_1 \tag{14}$$

where B_1 is the width of the section under evaluation, G_{1w} represents the self-weight of the wall above the section, E_{1x} and E_{1y} denote the horizontal and vertical components of the active earth pressure above the section; Z_{1w}, Z_{1x} and Z_{1y} refer to the moment arm lengths created by G_{1w}, E_{1x} and E_{1y}, respectively, at the intersection of the section and the wall face. Finally, f_1 refers to the friction coefficient of the wall material.

2.3 Optimum design problem formulation

Optimum design problems require explicit design variables, objective function and constraints. For the optimum design of railway gravity retaining walls, the inclination of the wall back and bottom are described using the tangent values of α and α_o, respectively. And a negative value of tanα indicates a landward-leaning wall back, while a zero value signifies vertical back, and a positive value indicates an outward-leaning inclination. Then, five parameters: n, tanα, b, tanα_o and b_1, are considered as design variables to determine the geometry of wall. If the angle β shown in Fig. 2b, is not greater than 45°, no bending and shear stresses need to be checked at the wall toe. By setting the toe step face slope at 1:n and $\beta=45°$, the value of h_1 can be obtained as $b_1/(1-n)$. Empirically, the following design variables were determined: $n\in[0, 0.35]$, tan$\alpha\in[-0.25, 0.25]$, $b\in[0.2, 0.625H]$, tan$\alpha_o\in[0, 0.20]$ and $b_1\in[0, H/20]$. The objective function is defined as the cross-sectional area of the retaining wall, and the optimum design solution should have the minimum cross-sectional area S_w. The constraints for the optimal design of the general regions are that: K_c, K_c', K_0, e, p_1, p_2, p_m, e_1, $\sigma_{1,2}$, $\sigma_{\max}$ and τ satisfy the

requirements specified in Table 1. In the table, $[\sigma_c]$ represents the compressive strength of the retaining wall material and $[\tau]$ denotes the shear strength. The bearing capacity σ_0 of ground and other parameters such as H_s, φ, f, d_s, that determine the working scenario of the retaining wall, can be input into the optimum design model as known design constants.

Table 1. Performance criteria used in gravity retaining wall design

Potential failure mode		Performance criteria
Instability	Sliding	$K_c \geq 1.3$; $K_c' \geq 1.3$
	Overturning	$K_0 \geq 1.6$
	Eccentricity	$e \leq B/4$ for unweathered or weakly weathered hard rock; $e \leq B/6$ for other condition.
	Bearing capacity (p_1, p_2, or p_m)	$p_1 \leq \sigma_0$; $p_2 \leq 1.3\sigma_0$; $p_m \leq \sigma_0$
Insufficient wall strength	Eccentricity	$\lvert e_1 \rvert \leq 0.3B_1$
	Normal compressive or tensile stress	$\lvert \sigma_{1,2} \rvert \leq [\sigma_c]$ and $[\sigma_t]$
	Maximum normal compressive stress	$\sigma_{max} \leq [\sigma_c]$
	Shear stress	$\tau \leq [\tau]$

The optimum design of the retaining wall is achieved using the FPA. The flowchart is illustrated in Fig. 3 and the steps are as follows:

Step 1: Parameter input. Enter the values of the parameters σ_0, H_s, φ, f, and d_s that define the working scenario in which the retaining wall will be employed. Additionally, specify the parameters p, n_{pop}, λ, γ, and the maximum number of iterations of the FPA algorithm.

Step 2: Initialization. In order to make the initial solution have a value of b while satisfying the constraints, n, $\tan\alpha$, $\tan\alpha_o$ and b_1 for each solution vector are generated randomly. The initial minimum value of b is then set as b_{min} = 0.2 m, and the initial maximum value of b is set as $b_{max} = 0.625H$. The retaining wall is then checked at $b=(b_{max}+b_{min})/2$. If the check passes, b_{max} is updated to b, and if it fails, b_{min} is updated to b, until convergence ($b_{max} - b_{min} \leq 0.001$ m). The initial solution that do not

satisfy the constraints are flagged, and unflagged in subsequent iterations if an optimal design solution emerges, to identify scenarios for which no solution exists. Subsequently, the solution exhibiting the smallest cross-sectional area is identified as the global optimal solution g^*.

Step 3: Pollination. For each design solution X_i^t, a random number is generated within the range of [0, 1], and subsequently compared to the switch probability p. In the event that the random number is smaller than p, a fresh solution X_i^{t+1} is produced through global pollination, as exemplified by Eq. 1. Conversely, if the random number is not less than p, a new solution X_i^{t+1} is generated through local pollination, as elucidated by Eq. 2.

Step 4: Evaluation. if the newly obtained solution X_i^{t+1} meet the stability and strength requirements, while also possessing a wall cross-sectional area $S_{w,i}^{t+1}$ that is smaller than $S_{w,i}^t$ of the original solution X_i^t, then X_i^t should be substituted with X_i^{t+1}. Otherwise, X_i^t remains unchanged. Further, if $S_{w,i}^{t+1}$ is smaller than the cross-sectional area of current global optimal solution g^*, then g^* is replaced by X_i^{t+1}.

Step 5: Termination. Revisit steps 3 and 4 until the maximum number of iterations is satisfied, and the global optimum is output.

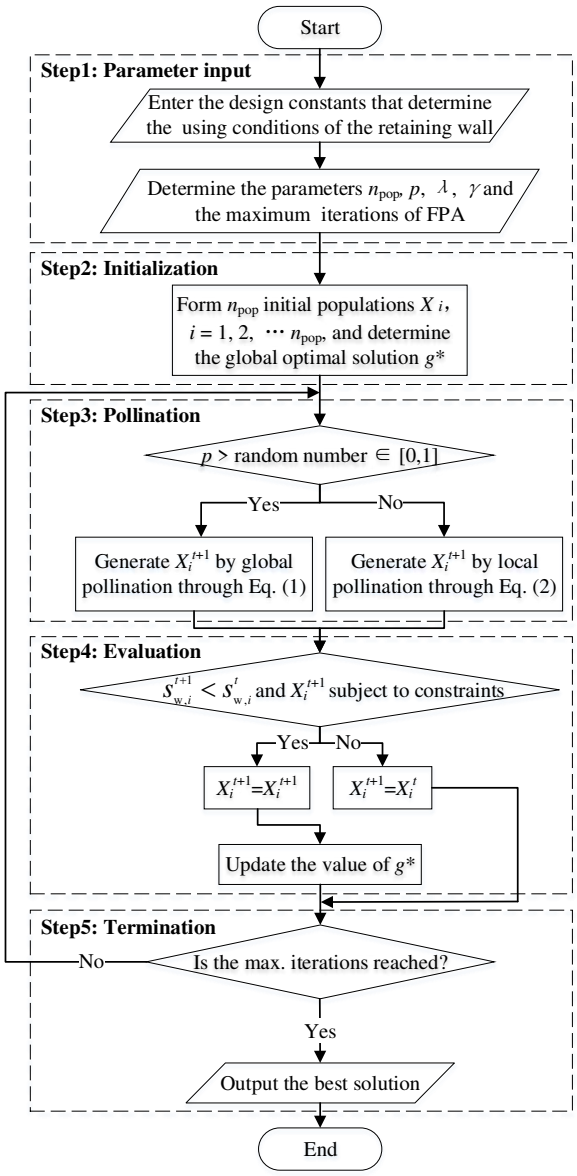

Fig. 3 Flowchart of optimum design of gravity retaining wall by FPA

3 Case study

In this section, a high-speed railway retaining wall is used as study case. First, the original design solution is compared with the FPA optimization results, and the FPA parameters such as p, n_{pop}, λ, and γ are tuned to explore the reasonable values in the optimal design of retaining walls. In addition, FPA is compared with GA, PSO, SSOA, and TWO algorithms to further evaluate the performance of FPA in this study.

3.1 Optimization results

The case utilizes a concrete slab track, with parameters d = 4.3 m, b_t = 3.1 m, D = 5 m, q_1=13.7 kN/m^2, q_2 = 40.4 kN/m^2 and q_0 =2.3 kN/m^2. The original design plan employed C30 concrete for the retaining wall, while the embankment soil has average weight γ_s = 20 kN/m^3, φ = 35°, and gravel ground has γ_g = 19 kN/m^3, σ_0 = 300 kPa, f' = 0.7. In addition, $\delta = \varphi/2$ and f = 0.38 were determined respectively at the back and bottom of the wall. And the scheme determined d_s = 5.8 m and H_s = 7 m. Optimized design from FPA adopts the same design parameters as the original plan. The comparison of the design solutions before and after optimization is shown in Fig. 4. In addition, the C30 concrete parameters, including γ_c = 23 kN/m^3, [σ_c] = 10 MPa, [σ_t] = 0.55 MPa, [τ] = 1.1 MPa, are determined according to the design code.

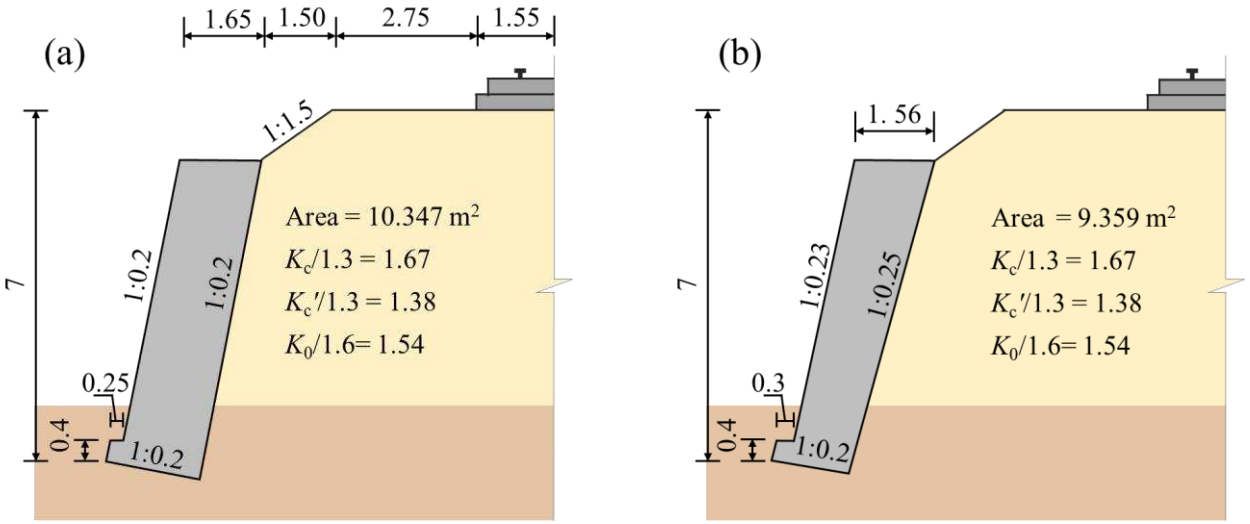

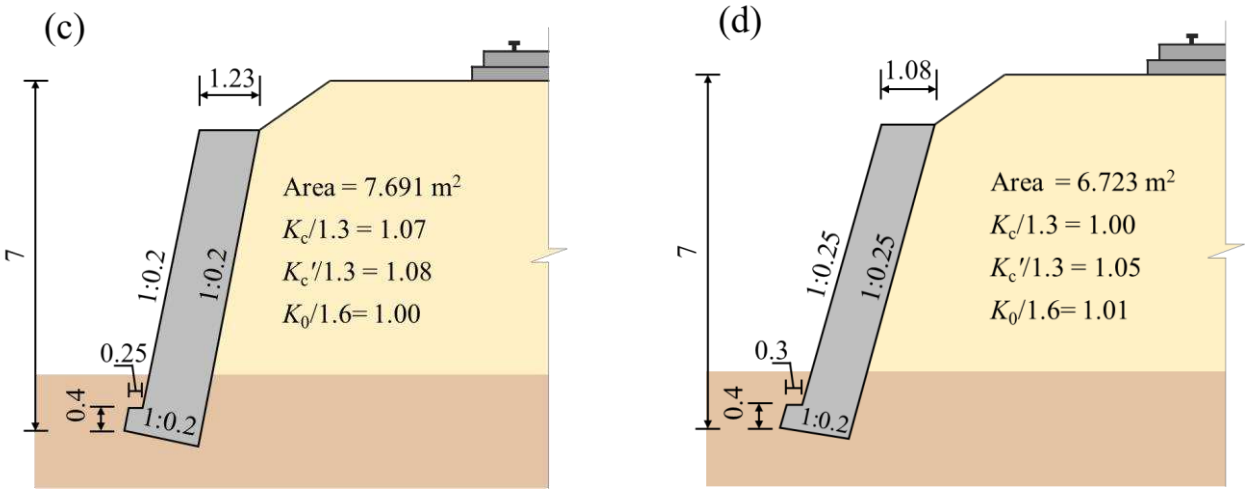

Fig. 4 Comparison of design schemes (Unit: m): (a) original design configuration; (b) FPA optimization with the same stability coefficient as the original design; (c) reduced wall width of the original design while meeting design requirements; (d) FPA global optimization while satisfying design requirements

All four design options shown in Fig. 4 meet the design requirements for wall strength, as well as eccentricity and stress at the bottom of the wall. The original design in Fig. 4a has a safety margin exceeding the design requirements outlined in Table 1, with a cross-sectional area of wall measuring 10.347 m^2. Selecting the same stability coefficient as the original design, the optimized design employing FPA in Fig. 4b has a reduced cross-sectional area of 9.359 m^2, representing a reduction of approximately 9.55%. Subsequently, the thickness of the wall in the initial design is decreased to precisely align with the design specifications in Table 1, resulting in the scheme displayed in Fig. 4c. FPA is once again utilized to optimize the design according to design requirements, leading to the scheme depicted in Fig. 4d, wherein the cross-sectional area experiences a reduction of approximately 12.59%. The results demonstrate that FPA yields a significant optimization effect on the section design of gravity retaining walls employed in railways. It is worth noting that the best solutions presented in Fig. 4b and d derived after numerous FPA trials.

The finite difference method is employed to construct a plane strain numerical model, elucidating the force condition acting on railway gravity retaining wall and enabling an evaluation of its support capacity both before and after optimal design. The numerical model integrates the construction process within the simulation, adhering to the code-required minimum burial depth of 1.0 m for the designed retaining wall. The development and validation of the model can be found in Appendix A. Following the construction of the retaining wall and the embankment fill, two design loads, q_1 and q_0, representing the self-weight of the track structure and the load between two tracks, are applied to the embankment crest. Following this, train loading, labelled as q_2, is implemented and progressively increased in increments of 0.2-fold, signifying the enhanced value as q_{2a}. This process continues until a sudden increase of wall displacement signals structural instability.

The primary displacements of all four walls in Fig. 4 under q_{2a} manifest as rotation around the wall base. And the relationship between the incremental displacement at the wall top and q_{2a}/q_2 is shown in Fig. 5. Evidently, both the embankments supported by the pre- and post-optimization retaining walls can withstand surcharge loads greater than those stipulated by the design code. The post-optimization retaining walls, depicted in Fig. 4b and d, support embankments that can withstand maximum q_{2a} values of approximately 5.2 and 3.6 times the value dictated by the specifications, slightly exceeding those supported by the non-optimized walls. This suggests that the optimized retaining walls, subjected to the same constraints, are not only more economic in terms of wall material but also exhibit potentially superior support capacity compared to their non-optimized counterparts.

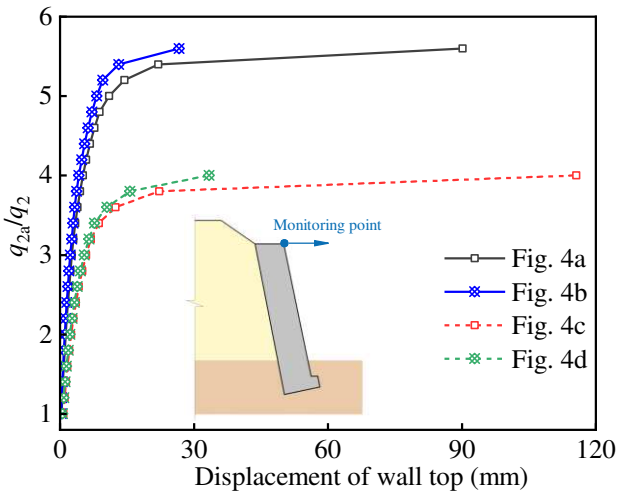

Fig. 5 Displacement of wall versus surcharge loads of embankment crest

3.2 FPA parameter tuning

As a preliminary investigation, it is crucial to investigate the impact of FPA parameters on the optimum design results of gravity retaining walls for railways. Specifically, the effects of p, n_{pop}, λ and γ will be probed herein. The influences of each parameter on the outcomes of ten runs after 2000 iterations are presented in Table 2, while their effects on the average iteration histories of the optimal design are illustrated in Fig. 6. The parameter values are adjusted based on the basic combination of p = 0.5, n_{pop} = 20, λ = 3/2 and γ = 0.01.

Table 2 displays the average, minimum, and maximum cross-sectional area obtained by the ten FPA runs, along with their corresponding coefficient of variation. The FPA algorithm produced promising predictions for most values of p, which range from 0 to 1.0 in increments of 0.1, as indicated by the minimum value of S_w. However, the quality of the outcomes deteriorates significantly for the extreme p values of 0 or 1.0, where the algorithm fails to combine global and local search to update the design variables. On the other hand, S_w values calculated by $p \in [0.1, 0.9]$ are better and more consistent. Moreover, the quality of the results further improves for p values ranging from 0.1 to 0.8.

In addition, Fig. 6a shows the average iteration histories generated by the FPA simulations using various values of p. It can be seen that a p value of 1.0 requires the greatest number of iterative steps to achieve convergence followed by a null value of p, which fails to fully exploit the performance of the algorithm. Although setting $p = 0.9$ gives acceptable results, FPA convergence requires about 800 iterations, which is significantly larger than 500 iterations needed for $p \in [0.1, 0.8]$. Further analysis of the optimisation results and computational efficiency reveals that the FPA performs well in finding the optimum design solution when the switch probability value p is within the range 0.1 to 0.8.

Table 2. FPA outcomes for different parameter values

Parameters	Values	Avg. S_w (m^2)	Max. S_w (m^2)	Min. S_w (m^2)	CoV (%)
p	0	7.196	8.031	6.781	5.53
	0.1	6.723	6.723	6.723	9.62e-04
	0.2	6.723	6.723	6.723	1.87e-04
	0.3	6.723	6.723	6.723	1.11e-04
	0.4	6.723	6.723	6.723	1.20e-04
	0.5	6.723	6.723	6.723	3.56e-04
	0.6	6.723	6.723	6.723	3.70e-04
	0.7	6.723	6.723	6.723	8.07e-04
	0.8	6.723	6.723	6.723	2.75e-03
	0.9	6.725	6.728	6.724	2.15e-02
	1.0	7.504	8.019	7.140	4.12
n_{pop}	10	6.723	6.723	6.723	1.51e-04
	20	6.723	6.723	6.723	3.56e-04
	30	6.723	6.723	6.723	9.79e-05
λ	1	6.723	6.723	6.723	2.99e-04
	3/2	6.723	6.723	6.723	3.56e-04
	2	6.723	6.723	6.723	1.45e-06
γ	0.001	6.723	6.723	6.723	7.73e-06
	0.01	6.723	6.723	6.723	3.56e-04
	0.1	6.723	6.723	6.723	2.57e-03
	1.0	6.725	6.741	6.723	8.52e-02

Note: CoV, Coefficient of variation.

Furthermore, Table 2 shows that the difference of the maximum S_w values obtained for n_{pop} = 10 to 30 is within 1‰ m^2, and this also holds true for the average and minimum S_w values. Additionally, the coefficients of variation for the results of multiple simulations are small, which shows that the population size has no significant influence on the optimal results. In addition, Fig. 6b illustrates the average iteration histories of S_w with different n_{pop} values. It is seen that all solutions converge almost to the same solution at approximately 300 iterations. However, convergence is still relatively slow at n_{pop} = 10. In contrast, the computational cost per iteration step increases significantly with a relatively large value of 30 for n_{pop}, without achieving better results or higher convergence efficiency. Therefore, it is recommended to set the value of n_{pop} to 20 when using the FPA method to optimize the design of gravity retaining walls.

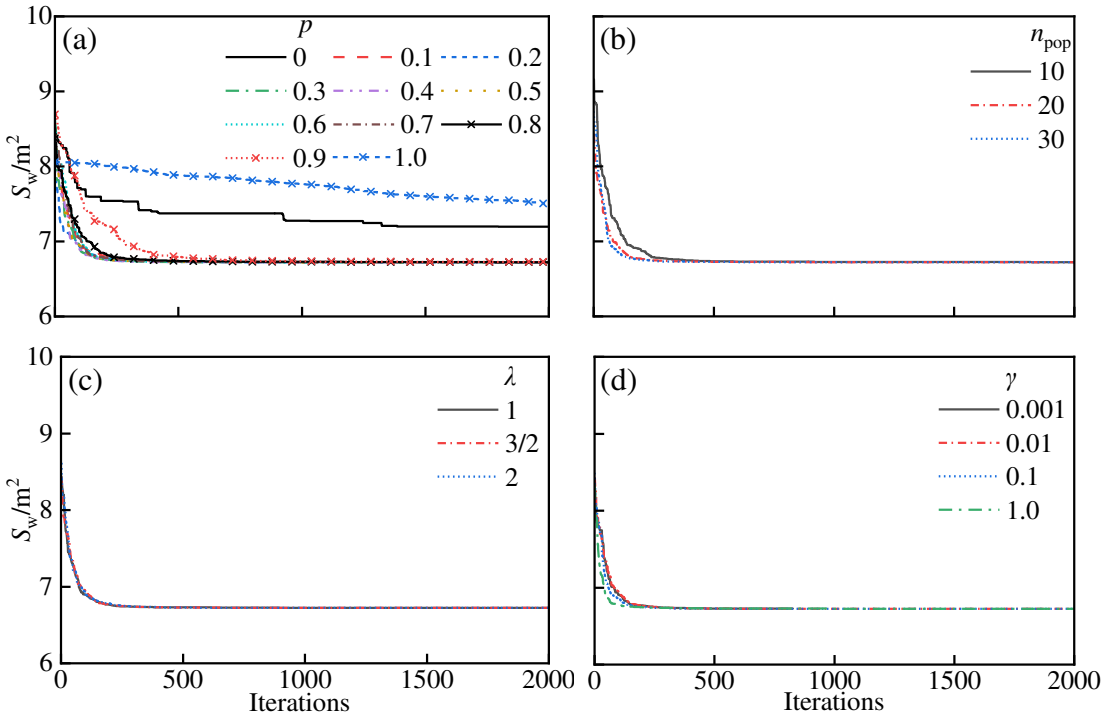

Fig. 6 Iteration histories for different parameter values: (a) p; (b) n_{pop}; (c) λ; (d) γ

Based on Table 2, it is apparent that optimal results can be achieved using λ values of 1, 3/2, and

2 after conducting 2000 iterations in the FPA simulations. Furthermore, Fig. 6c displays the average iteration histories of S_w with different λ values. It can be seen that the value of λ has almost no effect on the convergence efficiency.

In addition, the optimization results in Table 2 show that the outcomes for γ = 0.001 to 0.1 are superior compared to those for the larger value of 1.0. Moreover, Fig. 6d illustrates the average iteration histories of S_w with different γ values. It's observable that γ = 0.1 and 1.0 exhibit slightly faster convergence, but the overall variance in convergence efficiency across γ values is not significant. In light of the optimal results and efficiency, it was concluded to set γ in the range 0.001 to 0.1.

3.3 Comparison of optimization algorithms

The case study is also used to compare the performance of FPA with GA, PSO, SSOA and TWO in finding the optimum design. In a similar fashion to FPA, GA, PSO, SSOA and TWO are calculated with a population size of 20 individuals and 2000 maximum iterations. The MATLAB toolbox is utilized to implement the GA algorithm, with the default values being utilized for all parameters excluding the convergence criterion. PSO, on the other hand, makes use of the standard version as outlined by Kennedy [11]. In addition, parameters of SSOA and TWO tuned according to Kaveh's recommendations [36]. The parameters α_0, β_0, and β_{max} of SSOA are assigned the values 1.5, 2.0, and 2.5, respectively. Similarly, the parameters μ_s, α, and β of TWO take on the values 1.0, 0.99, and 0.01, respectively. In this context, the symbols of parameters for SSOA and TWO retain their original meanings as described in Ref. [36].The FPA parameters used for comparison are: p = 0.5, λ = 3/2, γ = 0.01.

Table 3 presents the statistical outcomes of 10 runs for various optimization methods. Each method

gives satisfactory results after several runs. However, compared to the GA, PSO, SSOA and TWO algorithms, the FPA algorithm shows higher convergence. The average iteration histories of S_w for each method are shown in Fig. 7. PSO, SSOA and TWO achieve an acceptable outcome after approximately 100 iterations, requiring a lower number of iterations. They are followed by the FPA at approximately 250 iterations, while GA requires the most iterations (approximately 800). Considering it's performance, the FPA method is a promising design optimization tool for the railway gravity retaining wall problem, and offers advantages in terms of convergence and number of iterations.

Table 3. Outcomes for different optimization methods

Method	Avg. S_w (m^2)	Max. S_w (m^2)	Min. S_w (m^2)	CoV (%)
FPA	6.723	6.723	6.723	3.56e-04
PSO	6.734	6.751	6.723	0.17
GA	6.728	6.742	6.723	0.09
SSOA	6.725	6.728	6.723	0.03
TWO	6.727	6.737	6.723	0.07

Note: CoV, Coefficient of variation.

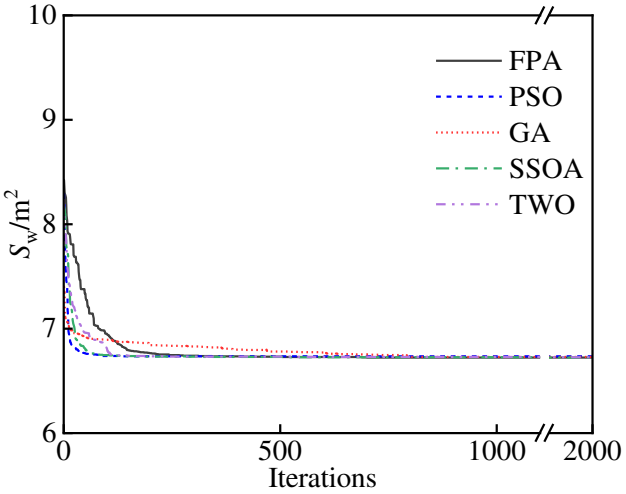

Fig. 7 Iteration histories for various optimization methods

4 Analysis

A parametric analysis was performed to study the effect of different design parameters on the

solution. Table 4 shows the design constants, σ_0, H_s, φ, d_s and f considered, resulting in 4,914 design permutations. An additional constraint was that the top of the wall is flush or slightly below the surface of the embankment, thus giving a wall height $H = H_s - h$, where $h = (d_s - 4.3\text{ m})/1.5$ for $d_s > 4.3$ m, and $h = 0$ for $d_s \leq 4.3$ m. Furthermore, the friction coefficient f' of the ground was approximated as $\tan(1.67\arctan f)$, while the other parameters were adopted from Section 3.1. Additionally, the retaining wall design was optimized for varying application scenarios using FPA, with the maximum number of iterations set to 1,000. n_{pop}, p, λ and γ were set to: 20, 0.5, 3/2 and 0.01, respectively. Each application scenario underwent three runs, and the optimal solution was chosen as the final outcome.

Table 4. Values of design constants associated with working scenarios

Design constants	Boundaries	Increment	Unit
σ_0	[100, 400)	50	kPa
	[400, 1000]	100	
H_s	[3, 9]	1	m
φ	[30, 40]	5	°
f	[0.3, 0.8]	0.1	—
d_s	[2.8, 5.3]	1.5	m

4.1 Design constraints

The results indicate that optimal solutions can be achieved when $\sigma_0 \geq 200$ kPa. However, certain scenarios did not yield solutions capable of meeting the design requirements (e.g., when σ_0 is 100 kPa or 150 kPa). This suggests that the gravity retaining wall design parameters under consideration are not suitable for supporting embankments under these particular conditions. Such scenarios that lack a solution vector are labelled in Fig. 8. This confirms that it is a challenging task to design a retaining wall for cases where σ_0 is low and H_s is high. For example, for scenarios where $\sigma_0 = 100$ kPa and $H_s \geq$

7 m, the preferrable design solution is likely to an alternatvie approach (i.e. not a gravity retaining wall). Similarly, gravity retaining walls that satisfy the problem constraints may not be attainable when H_s is 5 m or 6 m at σ_0 = 100 kPa, or when H_s is 8 m or 9 m at σ_0 = 150 kPa, particularly in cases where the wall is near to the track structure, the friction coefficient of wall-ground is insufficient or the friction angle of embankment fill is minimal.

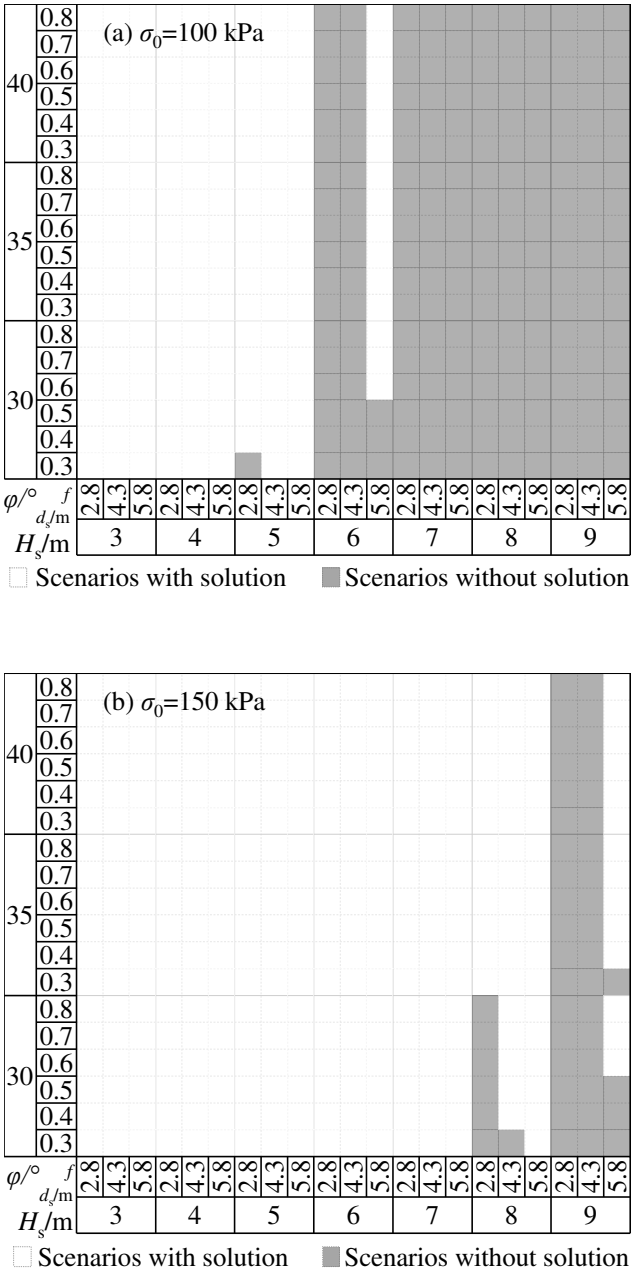

Fig. 8 Classification of scenarios based on the existence of solution vector: (a) σ_0 = 100 kPa; (b) σ_0 = 150 kPa

4.2 Sensitivity analysis

The root-mean-square (RMS) errors of the training results of the ANFIS model were compared for each input variable, with the aim of assessing the most influential variables [23,37]. The scenarios without a solution in Fig. 8 were omitted from the analysis, and the remaining data were then divided into training and checking sets, with the latter accounting for 30% of the data. Subsequently, MATLAB's "exhsrch" function was employed to investigate the relative importance of the design constants: σ_0, H_s, φ, f, and d_s, on S_w. The correspondence between the design constants and the RSM errors is presented in Fig. 9, with the variable or combination of variables on the upper side exhibiting the lowest errors and having the greatest influence on S_w.

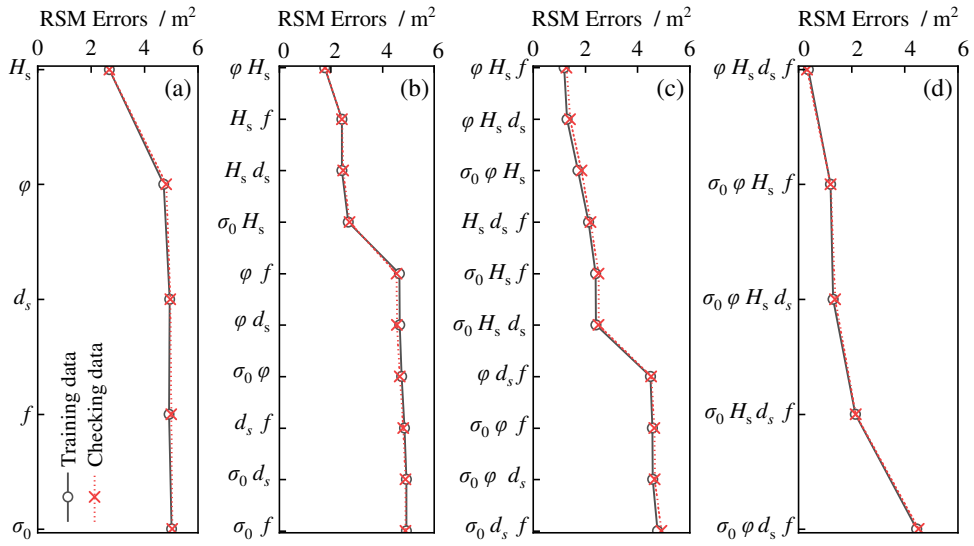

Fig. 9 Correspondence between the design constants and RSM errors: (a) single input variable; (b) all two input variable combinations; (c) all three input variable combinations; (d) all four input variable combinations

Fig. 9a illustrates that H_s is the most critical parameter for S_w, followed by φ, d_s, f, and finally σ_0 in descending order of importance. Single-factor analysis shows that the training and checking RSM errors are comparable, indicating the absence of overfitting and suggesting that the interplay of

multiple factors on S_w can be further explored. As observed in Fig. 9b-d, the RMS errors decrease with an increase in the number of input parameters, and the combination of "φ, H_s, d_s, f" yields the smallest errors and proves to be the most influential for S_w. It can be inferred that the interaction of multiple design constants significantly affects S_w, however σ_0 has only a weak correlation with S_w.

Assuming σ_0 = 1000 kPa as a reference value, the relative differences in S_w between other values of σ_0 and the reference value were calculated for each usage scenario, and the relationship between their distribution and σ_0 is depicted in Fig. 10. For $\sigma_0 \geq 300$ kPa, the relative difference in S_w falls within the range of [-0.5%, +5.0%], with an average value close to zero. Especially, for $\sigma_0 \geq 350$ kPa, the relative difference of S_w is confined to a narrow range of [−0.5%, +1.0%]. This suggests that when the bearing capacity of the ground is greater than 300 kPa, it does not impact the optimal design outcomes of the wall cross-sectional area. For $\sigma_0 < 300$ kPa, S_w exhibits a significant increase for higher Hs values compared to the reference conditions, leading to a noticeable increase in the relative difference of S_w. However, the mean increase remains below 5.0%. It can be seen that the correlation between S_w and σ_0 is limited.

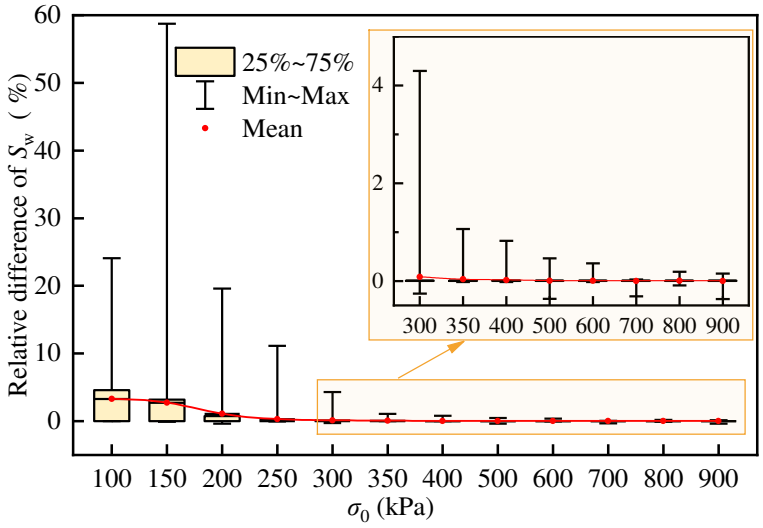

Fig. 10 Relationship between relative difference distribution of S_w and σ_0

Fig. 11 shows the distribution of S_w at different levels of each design constant. In Fig. 11a, an increase in H_s implies a taller embankment and gravity retaining wall, thus requiring a larger S_w to support and stabilize the soil behind the wall. An increase of φ leads to a reduction in the active earth pressure behind the wall, whereas a larger value of f can improve the resistance of the wall to slip instability. Moreover, a greater d_s can mitigate the impact of track and train loads on wall. Therefore, S_w in Fig. 11b-d decreases overall as the values of φ, f, and d_s increase. Notably, in Fig. 11e, S_w associated with lower values of σ_0 (100 kPa and 150 kPa) is considerably smaller than the scenarios where σ_0 is higher, due to the exclusion of unviable scenarios for large H_s. In addition, the distribution pattern of S_w at $\sigma_0 \geq 300$ kPa shows similarity, which is consistent with the previous discussion.

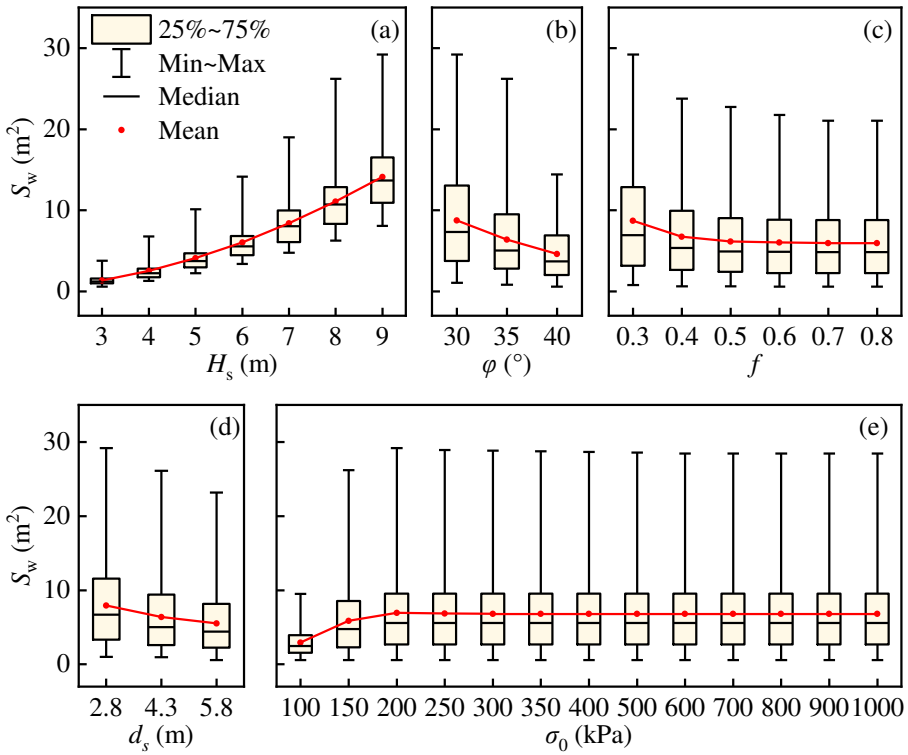

Fig. 11 Distribution of S_w at different values of (a) H_s; (b) φ; (c) f; (d) d_s; (e) σ_0

4.3 Analysis of design variables

The optimization results [5] demonstrate that the inclination of gravity retaining wall back in the

optimal design solution consistently corresponds to the given lower boundary [23]. Further analysis of the optimization results for the railway gravity retaining wall reveals that the optimal design solutions for 97.8% of the working scenarios have $\tan\alpha \in [-0.25, -0.24]$, which is approximately the same as the lower limit value. The optimal solutions for the working scenarios with $\tan\alpha > -0.24$ are adjusted by setting $\tan\alpha = -0.25$, and the optimization processes are performed again. It is found that the optimal design solution with $\tan\alpha = -0.25$ could solely not be obtained in a limited number of scenarios characterized by $\sigma_0 = 100$ kPa and $H_s = 5$ m, as well as $\sigma_0 = 150$ kPa and $H_s = 7$ m or 8 m, accompanied by considerably small values of f and d_s. In addition, the S_w of the optimal solution, achieved by adjusting the $\tan\alpha$ value to −0.25 for the remaining scenarios, exhibits a modest increase of no more than 2.0% compared to that obtained with unmodified $\tan\alpha$ value. This observation implies that the design of the railway retaining wall, featuring a landward-leaning back with a inclination angle of 14.04° ($\tan\alpha = -0.25$), aids in achieving the proper minimum cross-sectional area.

No statistically significant patterns were identified for the other design variables of optimal design solution. However, it is believed that the following analysis can still serve as a useful reference for engineers in determining a more rational design solution. The relationship between the width of the toe step and the height of the retaining wall is denoted by b_1/H, while the relationship between the width of the wall top and the height of the wall is expressed as b/H. By employing the "exhsrch" function, it is evident that the the friction coefficient f of the wall-ground exerts the most substantial influence on n, $\tan\alpha_o$, b_1/H, and b/H of optimization results. Consequently, the discussion primarily revolves around the influence of varying values of f on n, $\tan\alpha_o$, b_1/H, and b/H of optimal design solution, as depicted in Fig. 12.

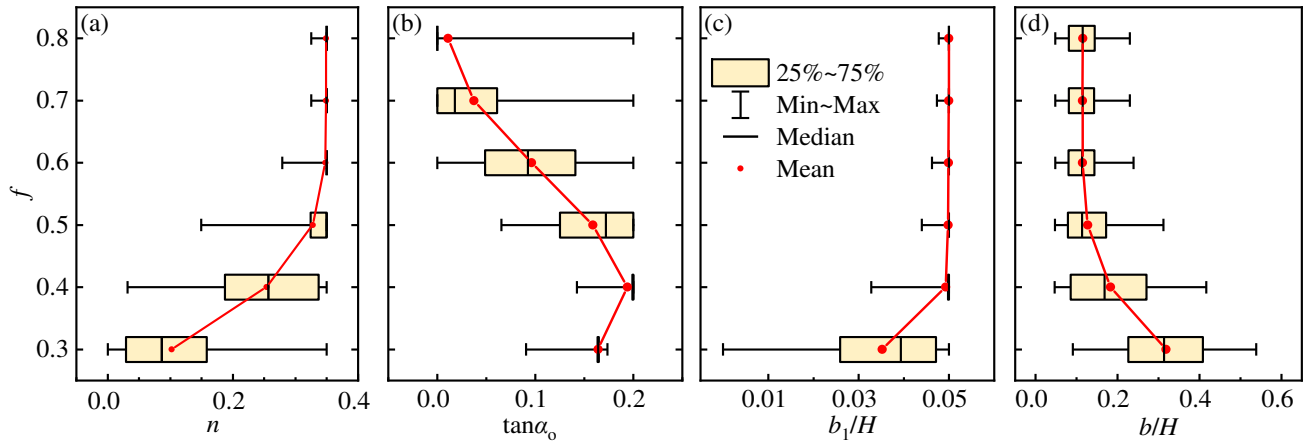

Fig. 12 Distribution of (a) n, (b) $\tan\alpha_o$, (c) b_1/H, and (d) b/H at different values of f

As shown in Fig. 12a, the average magnitude of n exhibits an ascending trend as f escalates, indicating that heightened wall-ground friction leads to a more gradual inclination of the wall face for optimal design solution. Moreover, it is imperative to note that the optimal design solution should have $n = 0.35$ for a substantial majority of scenarios wherein the value of f does not fall below 0.6. In Fig. 12b, for a diminutive f value of 0.3, the friction of the ground soil is low. Consequently, the design of the retaining wall is predominantly controlled by the potential slip surface along the horizontal plane where the wall heel is located. In these scenarios, the most suitable design solution for the majority of applications corresponds to a $\tan\alpha_o$ value of approximately 0.165. For $f \geq 0.4$, the optimal design solution of retaining wall is independent of ground soil strength. As f increases, gentle bottom surface of wall can offer sufficient resistance against slip through wall-ground friction. Consequently, the mean $\tan\alpha_o$ decreases with increasing f. In addition, the optimal solutions for most scenarios with $f = 0.4$ and $f = 0.8$ correspond to $\tan\alpha_o$ values of 0.2 (upper limit) and 0.01 (approximate horizontal surface), respectively.

Fig. 12c demonstrates a larger distribution and smaller mean value of b_1/H for the optimal design

solution when $f = 0.3$. However, when $f \geq 0.4$, b_1/H converges around 0.05, indicating that obtaining a design solution with a smaller cross-sectional area is easier when the wall toe step width is 1/20 of the wall height. Fig. 12d reveals that, as f increases, the mean value of b/H for the optimal design solution generally decreases. Once f surpasses 0.6, the b/H distribution remains largely unaffected by further changes in f. During this stage, the optimal design solution corresponds to a wall top width ranging from approximately 0.05 to 0.23 times the wall height.

5 Conclusions

The design of railway gravity retaining walls using conventional methods can often pose challenges in achieving optimal cross-sectional areas. In this study, the flower pollination algorithm (FPA) is employed to address this issue and find a design solution that meets the design requirements with a minimum cross-sectional area S_w. The performance of FPA in optimizing retaining walls is explored through a case study on high-speed railway. Furthermore, a parametric analysis is conducted to examine the impact of design parameters on S_w where the top of the wall is flush with, or slightly below the embankment crest. The main conclusions can be summarized as follows:

(1) The FPA approach was successful in finding solutions that met the design requirements while minimising the cross sectional area of the retaining wall. Detailed analysis showed that the value of S_w is influenced by the relationship between height H_s of the wall toe from the embankment crest, the friction angle φ of the fill behind the wall, the distance d_s between the highest point of the wall back and the centre line of the track near the wall, and friction coefficient f of the wall-ground. H_s exerts the greatest influence on S_w, followed by φ, d_s, f and ground bearing capacity σ_0. Further, H_s exhibits a positive correlation with S_w, while φ, d_s and f display a negative correlation. Also, the average relative

difference in S_w remains below 5.0% when σ_0 is reduced compared to σ_0 = 1000 kPa for every combination of H_s, φ, d_s, and f. Lastly, S_w is insensitive to σ_0 values of 300 kPa or greater.

(2) Design variables selection critically influences the development of design strategies that minimize the cross-sectional area for retaining walls. Statistical scrutiny of these strategies reveals the utility of a specific railway retaining wall blueprint, distinguished by a landward-leaning wall back at an inclination angle α of 14.04° ($\tan\alpha = -0.25$), in achieving minimum cross-sectional dimensions. Furthermore, f significantly influences other design variables. A wall face slope of 1:0.35 becomes beneficial for constructing optimal designs when $f \geq 0.6$, and in such optimal designs, the wall top width approximates 0.05 to 0.23 times the wall height. Moreover, under the majority of working scenarios where $f \geq 0.4$, the optimal design solution approximates the toe step width to be 1/20 of the wall height. Furthermore, selecting $\tan\alpha_o$—where α_o is the angle between the bottom surface of wall and the horizontal plane—as 0.165, 0.2, or 0.01 when f equals 0.3, 0.4, or 0.8, respectively, facilitates the achievement of the minimal cross-sectional area for the retaining wall.

(3) For certain simulation permutations it was found that a gravity retaining wall was not a viable design solution, in particular for problems with a low σ_0 and a high H_s. More specifically, gravity retaining wall solutions could not be found when σ_0 = 100 kPa and $H_s \geq 7$ m. Furthermore, the attainment of an appropriate design solution may be impeded by constraints such as H_s = 5 m or 6 m at σ_0 = 100 kPa, or H_s = 8 m or 9 m at σ_0 = 150 kPa, particularly in cases where the retaining wall is in close proximity to the track structure, the friction of the wall-ground is deficient, or the friction angle of the embankment fill behind the wall is insufficient.

(4) Parametric investigations are undertaken to identify the FPA parameters that yield peak

performance of this algorithm for the optimization problem. It is found that switch probability values within the range of 0.1 and 0.8, a population size of 20, a constant of the Lévy flight step size in the span of 1 and 2, and a Lévy flight step size scale factor between 0.001 and 0.1 yield the optimum performance in terms of both obtaining smallest cross-sectional area and convergence performance.

(5) The efficiency of FPA in solving the optimization problem of this study is compared with GA, PSO, SSOA, and TWO algorithms. All the algorithms can obtain the optimum design solution for the retaining wall after several runs. However, FPA has better consistency in the results obtained from repeated runs than the latter four, and requires fewer iterations to converge to the ideal result than the GA algorithm. Furthermore, numerical models suggest that design solutions derived from optimization strategies demonstrate a potential superiority in support capacity compared to their non-optimized counterparts.

It should be noted that this paper allows for the minimisation of cross-sectional areas, but this might not always lead to the minimum costs, for example because different design solutions may require different construction methods. Also, some projects may be more concerned with construction duration (e.g. a railway where the construction needs completed rapidly before operation), sustainability, or resilience against future climate conditions in comparison to cross-sectional area. Furthermore, the constraints within the optimization methodology employed in the paper solely address the stability and strength requirements of the wall in accordance with the prevailing design codes. However, this approach does not incorporate the deformation of embankment fill behind the wall. Such deformation plays a crucial role in relation to the operational state of the train and the long-term durability performance of the track and embankment. In light of this, although this research aims

to guide the design of railway gravity retaining walls, it acknowledges the possible need for further adjustments for real-life application.

Acknowledgments

This work was supported by the National Natural Science Foundation of China under grant number 52078435; the Natural Science Foundation of Sichuan Province under grant number 2023NSFSC0391; and the 111 Project under grant number B21011.

Appendix A

A1. Model development

The analysis of the support capacity of railway gravity retaining wall is abstracted as a plane strain problem. The numerical model conservatively considers only the semi-embankment symmetrical to the line center, with each structural component simulated by solid elements. The fill within the embankment incorporates a stratified structure, comprising, in descending order, an upper trackbed, a lower trackbed, and subgrade. Interactions between the soil and the wall are simulated through the use of interface elements, with shared grid points at the position of contact between each soil layer. In reference to Fig. 4a within the main text, the numerical model constructed for the embankment is depicted in Fig. A1. The upper trackbed measures 0.4 m, the lower trackbed is 2.3 m, and the model encompasses 2,632 elements and 2,774 grid points in total. In addition, roller boundaries are implemented for the lateral sides, while pinned boundaries are utilized for the bottom of the model.

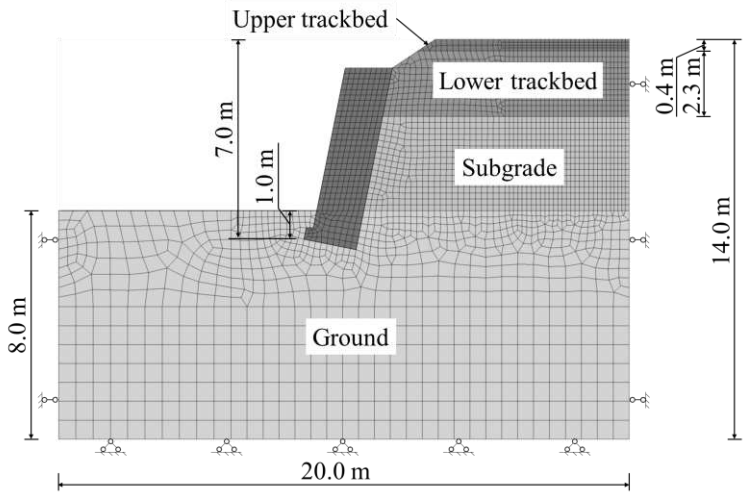

Fig. A1 Meshes and configuration of the numerical model

The numerical simulation process duly incorporates the construction sequence. Initially, a geological model is crafted, and a geostatic stress field is cultivated during the site conditioning phase. The subsequent stage involves the assembly of the retaining wall and emplacement of backfill, with both displacement and velocity fields being nullified upon convergence. The penultimate phase mimics the implementation of an evenly distributed load, epitomizing the self-weight of the tracks and the load interposed between them, subsequently leading to the computation of the stress field. Ultimately, a uniformly distributed load symbolizing the influence of the train is imposed and is gradually amplified to probe the stability status of the retaining wall.

The concrete constituting the retaining wall structure in the model is delineated as a linearly elastic material, while the soils employ an ideal elastoplastic model adhering to the Mohr-Coulomb failure criterion, with Table A1 for material properties. Pertaining to soils, the deformation modulus (E) is employed under the influence of structural self-weight, whereas the elastic modulus (E_d) is used to ascertain the consequences of train loadings. Luo et al. [38] proposed that the modulus of subgrade reaction (K_{30}) can serve as an effective estimator for both E and E_d. In these cases, the K_{30} values of

the upper trackbed, lower trackbed, and subgrade are respectively designated as per the recommended limit values of 190 MPa/m, 150 MPa/m, 130 MPa/m, as stipulated by the *Code for Design of Railway Earth Structure* (TB10001-2016).

Table A1. Material properties of numerical model

Component	Material	Density ρ (kg·m^{-3})	Deformation modulus E (MPa)	Elastic Modulus E_d (MPa)	Poisson's ratio μ	Friction angle φ (°)
Retaining wall	C30 concrete	2,300	—	30,000	0.20	—
Upper trackbed	Graded gravel	2,100	41.9	214.0	0.25	41.8
Lower trackbed	Class-A, B fill	2,050	32.2	168.6	0.30	35.0
Subgrade	Class-A, B, C fill	2,000	27.8	147.8	0.30	34.5
Ground	Coarse-grained soil	2,000	25.4	135.8	0.30	34.2

Utilising Eq. 15, which establishes a relationship between the ground's bearing capacity (σ_0) and K_{30} [39], an interconnection between E, E_d, and σ_0 can be delineated. The friction angle (φ) for coarse-grained ground soil can be characterised by a statistical relationship with σ_0, as manifested in Eq. 16, with data fitting this formulation derived from the *Technical Code for Building Foundation* (DB21/T 907-2015). Regarding the scenarios depicted in Fig. 4, the φ of ground is estimated to be 34.18° using Eq. 16 with σ_0 equating to 300 kPa, and it closely matches the value of 34.99° (arctan f ')utilised in stability analysis.

$$K_{30} = 0.42\sigma_0 - 6.25 \tag{15}$$

where K_{30} and σ_0 are expressed in units of MPa/m and kPa, respectively.

$$\varphi = 0.0166\sigma_0 + 29.2 \tag{16}$$

where φ and σ_0 are both measured in degree and kPa, respectively.

The coefficient of earth pressure at rest ($K_{h,0}$) in normally consolidated soil exhibits an approximate correlation with the soil friction angle φ, as indicated by Eq. 17 [40]. Moreover, Eq. 18 [41] shows the relationship between $K_{h,0}$ and Poisson's ratio μ under the assumption of elasticity.

Subsequently, Eq. 19 can be derived to provide an approximation for the connection between μ and φ. Additionally, an associated flow rule is employed in the calculations.

$$K_{\mathrm{h},0} = 1 - \sin\varphi \tag{17}$$

$$K_{\mathrm{h},0} = \frac{\mu}{1-\mu} \tag{18}$$

$$\mu = \frac{K_{\mathrm{h},0}}{1+K_{\mathrm{h},0}} = \frac{1-\sin\varphi}{2-\sin\varphi} \tag{19}$$

A2. Model validation

The validity of numerical model is established through verification with an in-situ test documented by Feng et al. [42], derived from a railway cross-section depicted in Fig. A2. And the materials' parameters of numerical model are also indicated in Fig. A2. Furthermore, the track and train loading in the simulation adhere to the guidelines stipulated by the *Code for Design of Retaining Structures of Railway Earthworks* (TB10025-2019). According to the recommendations, q_1 is to be set at 17.3 kN/m^2, q_2 at 55.2 kN/m^2, with a distribution width of 3.4 m.

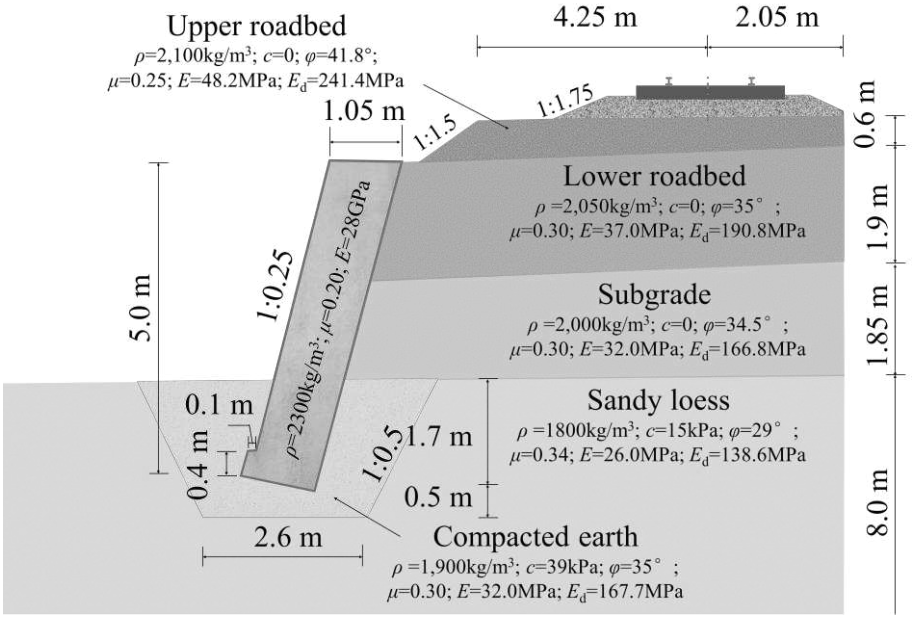

Fig. A2 Cross-section of in-situ test and parameters of numerical model

Fig. A3 illustrates the comparison, with calculated values of earth pressure due to self-weight of structure and train loading approximately matching the measured values in magnitude and trend. The consistency implies that the numerical model is suitable for analyzing the force of railway gravity retaining wall.

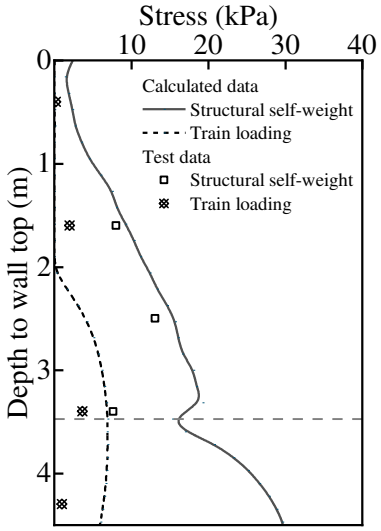

Fig. A3 Comparison between calculated and test data for earth pressure against the retaining wall

References

[1] Roshan MJ, A Rashid AS, Abdul Wahab N, Tamassoki S, Jusoh SN, Hezmi MA, et al. Improved methods to prevent railway embankment failure and subgrade degradation: A review. Transportation Geotechnics 2022;37:100834. https://doi.org/10.1016/j.trgeo.2022.100834.

[2] Xu S, Zsáki AM. Maximum safe freight train speed on railway embankments under rapid drawdown conditions based on coupled stress-seepage slope stability analysis. Transportation Geotechnics 2021;27:100486. https://doi.org/10.1016/j.trgeo.2020.100486.

[3] Esen AF, Woodward PK, Laghrouche O, Connolly DP. Stress distribution in reinforced railway structures. Transportation Geotechnics 2022;32:100699. https://doi.org/10.1016/j.trgeo.2021.100699.

[4] Luo Q, Wei YX. High-speed railway roadbed. Beijing: China Railway Publishing House Co., Ltd; 2021.

[5] Chen DL, Dang JQ. Study on optimum cross-section of gravity retaining wall. Rock and Soil Mechanics 2007:1969–73. https://doi.org/10.16285/j.rsm.2007.09.039.

[6] Liu CQ, Li SY, Liu SF. Experimental Investigation of Dynamic Earth Pressure on Gravity Retaining Structures. Journal of Southwest Jiaotong University 2010;45:357-360+372. https://doi.org/10.3969/j.issn.0258-2724.2010.03.006.

[7] Xiao JZ, Xia B, Xiao XW, Li Y, Xue ST, Zhou Y, et al. Prospects for low-carbon design theory

of concrete structures. Chinese Science Bulletin 2022;67:3425–38. https://doi.org/10.1360/TB-2022-0055.
[8] Gandomi AH, Yang X-S, Alavi AH. Cuckoo search algorithm: a metaheuristic approach to solve structural optimization problems. Engineering with Computers 2013;29:17–35. https://doi.org/10.1007/s00366-011-0241-y.
[9] Yang XS. Firefly algorithm, stochastic test functions and design optimisation. IJBIC 2010;2:78–84. https://doi.org/10.1504/IJBIC.2010.032124.
[10] Holland JH. Adaptation in natural and artificial systems . An introductory analysis with applications to biology, control and artificial intelligence. University of Michigan, Ann Arbor: 1975.
[11] Kennedy J. Particle Swarm Optimization. In: Sammut C, Webb GI, editors. Encyclopedia of Machine Learning, Boston: Springer; 2011, p. 760–6. https://doi.org/10.1007/978-0-387-30164-8_630.
[12] Kaveh A, Zaerreza A. Shuffled shepherd optimization method: a new Meta-heuristic algorithm. EC 2020;37:2357–89. https://doi.org/10.1108/EC-10-2019-0481.
[13] Kaveh A, Zolghadr A. A novel meta-heuristic algorithm: tug of war optimization. Int J Optim Civil Eng 2016;6:469–93.
[14] Kaveh A, Talatahari S. A novel heuristic optimization method: charged system search. Acta Mech 2010;213:267–89. https://doi.org/10.1007/s00707-009-0270-4.
[15] Yang XS. Flower pollination algorithm for global optimization. Unconv Comput Nat Comput 2012;7445:240–9.
[16] Kaveh A, Mahdavi VR. Shape optimization of arch dams under earthquake loading using meta-heuristic algorithms. KSCE J Civ Eng 2013;17:1690–9. https://doi.org/10.1007/s12205-013-0463-1.
[17] Kaveh A, Biabani Hamedani K, Bakhshpoori T. Optimal Design of Reinforced Concrete Cantilever Retaining Walls Utilizing Eleven Meta-Heuristic Algorithms: A Comparative Study. Period Polytech Civil Eng 2020. https://doi.org/10.3311/PPci.15217.
[18] Kaveh A, Behnam AF. Charged System Search Algorithm for the Optimum Cost Design of Reinforced Concrete Cantilever Retaining Walls. Arab J Sci Eng 2013;38:563–70. https://doi.org/10.1007/s13369-012-0332-0.
[19] Konstandakopoulou FD, Tsimirika M, Pnevmatikos N, Hatzigeorgiou G. Optimization of Reinforced Concrete Retaining Walls Designed According to European Provisions. Infrastructures 2020;5:46. https://doi.org/10.3390/infrastructures5060046.
[20] Mergos PE, Mantoglou F. Optimum design of reinforced concrete retaining walls with the flower pollination algorithm. Struct Multidisc Optim 2020;61:575–85. https://doi.org/10.1007/s00158-019-02380-x.
[21] Pei YY, Xia YY. Design of Reinforced Cantilever Retaining Walls using Heuristic Optimization Algorithms. Procedia Earth and Planetary Science 2012;5:32–6. https://doi.org/10.1016/j.proeps.2012.01.006.
[22] Yücel M, Bekdaş G, Nigdeli SM, Kayabekir AE. An Artificial Intelligence-Based Prediction Model for Optimum Design Variables of Reinforced Concrete Retaining Walls. International Journal of Geomechanics 2021;21:04021244. https://doi.org/10.1061/(ASCE)GM.1943-

5622.0002234.
[23] Varga R, Žlender B, Jelušič P. Multiparametric Analysis of a Gravity Retaining Wall. Applied Sciences 2021;11:6233. https://doi.org/10.3390/app11136233.
[24] Talatahari S, Sheikholeslami R, Shadfaran M, Pourbaba M. Optimum Design of Gravity Retaining Walls Using Charged System Search Algorithm. Mathematical Problems in Engineering 2012;2012:e301628. https://doi.org/10.1155/2012/301628.
[25] Kaveh A, Zakian P. Stability based optimum design of concrete gravity dam using CSS, CBO and ECBO algorithms. International Journal of Optimization in Civil Engineering 2015;5:419–31.
[26] Alyasseri ZAA, Khader AT, Al-Betar MA, Awadallah MA, Yang X-S. Variants of the Flower Pollination Algorithm: A Review. In: Yang X-S, editor. Nature-Inspired Algorithms and Applied Optimization, Cham: Springer International Publishing; 2018, p. 91–118. https://doi.org/10.1007/978-3-319-67669-2_5.
[27] Emary E, Zawbaa HM, Hassanien AE, Parv B. Multi-objective retinal vessel localization using flower pollination search algorithm with pattern search. Adv Data Anal Classif 2017;11:611–27. https://doi.org/10.1007/s11634-016-0257-7.
[28] Ouadfel S, Taleb-Ahmed A. Social spiders optimization and flower pollination algorithm for multilevel image thresholding: A performance study. Expert Systems with Applications 2016;55:566–84. https://doi.org/10.1016/j.eswa.2016.02.024.
[29] Abdelaziz AY, Ali ES, Abd Elazim SM. Combined economic and emission dispatch solution using Flower Pollination Algorithm. International Journal of Electrical Power & Energy Systems 2016;80:264–74. https://doi.org/10.1016/j.ijepes.2015.11.093.
[30] Abdelaziz AY, Ali ES, Abd Elazim SM. Implementation of flower pollination algorithm for solving economic load dispatch and combined economic emission dispatch problems in power systems. Energy 2016;101:506–18. https://doi.org/10.1016/j.energy.2016.02.041.
[31] Nigdeli SM, Bekdaş G, Yang X-S. Application of the Flower Pollination Algorithm in Structural Engineering. In: Yang X-S, Bekdaş G, Nigdeli SM, editors. Metaheuristics and Optimization in Civil Engineering, Cham: Springer International Publishing; 2016, p. 25–42. https://doi.org/10.1007/978-3-319-26245-1_2.
[32] Singh J, Kumar R, Banka H. Application of Flower Pollination Algorithm to Locate Critical Failure Surface for Slope Stability Analysis. In: Das SK, Das SP, Dey N, Hassanien A-E, editors. Machine Learning Algorithms for Industrial Applications, Cham: Springer International Publishing; 2021, p. 301–15. https://doi.org/10.1007/978-3-030-50641-4_17.
[33] Öcal A, Sarıçiçek YE, Pekcan O. Flower Pollination Algorithm for Slope Stability Analysis. In: Dey N, editor. Applications of Flower Pollination Algorithm and its Variants, Singapore: Springer; 2021, p. 87–111. https://doi.org/10.1007/978-981-33-6104-1_5.
[34] Chittka L, Thomson JD, Waser NM. Flower Constancy, Insect Psychology, and Plant Evolution. Naturwissenschaften 1999;86:361–77. https://doi.org/10.1007/s001140050636.
[35] Bakr J, Ahmad SM. A finite element performance-based approach to correlate movement of a rigid retaining wall with seismic earth pressure. Soil Dynamics and Earthquake Engineering 2018;114:460–79. https://doi.org/10.1016/j.soildyn.2018.07.025.
[36] Kaveh A. Advances in Metaheuristic Algorithms for Optimal Design of Structures. Cham:

Springer International Publishing; 2021. https://doi.org/10.1007/978-3-030-59392-6.
[37] Jelušič P, Varga R, Žlender B. Parametric analysis of the minimum cost design of flexible pavements. Ain Shams Engineering Journal 2022:101840. https://doi.org/10.1016/j.asej.2022.101840.
[38] Luo Q, Zhang RG, Xie HW, Tian D. Structural Analysis and Key Parameter of Ballastless Track Subgrade for 400 km/h High Speed Railway. CHINA RAILWAY SCIENCE 2020;41:34–44. https://doi.org/10.3969/j.issn.1001-4632.2020.02.05.
[39] Kan SY, Chen YY, Zhou XJ. Heavy haul railway engineering. Beijing: China Railway Publishing House; 1994.
[40] JAKY J. The coefficient of earth pressure at rest. Journal of the Society of Hungarian Architects and Engineers 1944;78:355–8.
[41] TSCHEBOTARIOFF G P. Soil mechanics foundations and earth structures. New York: McGraw-Hill; 1951.
[42] Feng GS, Zhang L, Luo Q, Wang TF, Xie HW. Monitoring the dynamic response of track formation with retaining wall to heavy-haul train passage. International Journal of Rail Transportation 2022:1–19. https://doi.org/10.1080/23248378.2022.2103849.